Metals **2015**, *5*, 1829-1844; doi:10.3390/met5041829

OPEN ACCESS

metals

ISSN 2075-4701

www.mdpi.com/journal/metals/

Article

Effect of Polymer Addition on the Structure and Hydrogen Evolution Reaction Property of Nanoflower-Like Molybdenum Disulfide

Xianwen Zeng, Lijing Niu, Laizhou Song *, Xiuli Wang, Xuanming Shi and Jiayun Yan

College of Environmental and Chemical Engineering, Yanshan University, Qinhuangdao 066004, China; E-Mails: ydzxw7903@163.com (X.Z.); nljing0321@163.com (L.N.); xlwang7904@ysu.edu.cn (X.W.); sxming3231@163.com (X.S.); yanjiayun@163.com (J.Y.)

* Author to whom correspondence should be addressed; E-Mail: songlz@ysu.edu.cn; Tel./Fax: +86-335-8061569.

Academic Editors: Suresh Bhargava, Mark Pownceby and Rahul Ram

Received: 8 September 2015 / Accepted: 25 September 2015 / Published: 9 October 2015

Abstract: Nano-structured molybdenum disulfide (MoS_2) catalysts have been extensively developed for the hydrogen evolution reaction (HER). Herein, a novel hydrothermal intercalation approach is employed to fabricate nanoflower-like 2H–MoS_2 with the incorporation of three polymers, polyvinylpyrrolidone (PVP), polyvinyl alcohol (PVA), and polyethylenimine (PEI). The as-prepared MoS_2 specimens were characterized by techniques of scanning electron microscope (SEM), transmission electron microscopy (TEM), X-ray diffraction (XRD), together with Raman and Fourier transform infrared spectroscopy (FTIR). The HER properties of these lamellar nanoflower-like composites were evaluated using electrochemical tests of linear sweep voltammetry (LSV) and electrochemical impedance spectroscopy (EIS). The existent polymer enlarges the interlayer spacing of the lamellar MoS_2, and reduces its stacked thickness. The lamellar MoS_2 samples exhibit a promoting activity in HER at low additions of these three polymers (0.04 g/g MoS_2 for PVA and PEI, and 0.08 g/g MoS_2 for PVP). This can be attributed to the fact that the expanded interlayer of MoS_2 can offer abundant exposed active sites for HER. Conversely, high additions of the polymers exert an obvious interference in the HER activity of the lamellar MoS_2. Compared with the samples of MoS_2/PVP–0.08 and MoS_2/PEI–0.04, the MoS_2/PVA–0.04 composite exhibits excellent activity in HER, in terms of higher current density and lower onset potential.

Keywords: nanoflower-like molybdenum disulfide; hydrogen evolution reaction; polymer intercalation; electrochemical test

1. Introduction

Hydrogen as an ideal, clean and efficient secondary energy resource serves as one of the most competent candidates for replacing petroleum fuels for the future. The electrolysis of water is the most mature and promising method for the production of hydrogen [1,2]. Thus, a variety of nonmetal and metal materials such as carbides [3,4], and Pt-group alloys [5,6] employed as catalysts for the hydrogen evolution reduction (HER) have been extensively explored. Up to date, it has been difficult to push the industrial applications of them because of the poor activities in HER or high costs. Compared with the above-mentioned materials, chalcogenides [7–9], particularly, molybdenum disulfide (MoS_2), possess the merits of acceptable cost, acidic stability, easy fabrication, and a higher electrocatalytic property [10,11]. The suitability of MoS_2 as an excellent catalyst for HER, is mainly due to the catalytic activity at the edge of this lamellar crystal [7,12,13]. It has been proved by theoretical and experimental studies that the active sites of 2H-MoS_2 for HER locate the (010) and (100) planes with the existence of unsaturated molybdenum and sulfur atoms, while the (002) basal plane is inactive [7,12,14].

In general, there are three pathways to obtain MoS_2 catalyst with an effective activity in HER. They are briefly described as follows: (1) increase in the intrinsic activity of active sites, for instance, Ni, B, and Fe metals have been incorporated to improve the catalytic activity of MoS_2 [15,16]; (2) improvement in the electrical contact between the catalytic sites, such that graphite [17], mesoporous carbon [18], and reduced graphene oxide [19,20] have been employed to improve electrical conductivity; (3) enhancement in the number of active sites, thus the decrease in crystal size and stacked thickness have been taken into account. It is well known that the HER activity of MoS_2 decreases with the increase of stacked thickness, because of the Van der Waals force interactions within its interlayer [21–23]. Therefore, most studies in the electrocatalytic enhancements of MoS_2 have focused on improving the density of the active sites and reducing the stacked thickness. Based on this consideration, the chemical exfoliation process [24] and the low pressure chemical vapor deposition method [25] were employed for the fabrications of exfoliated 1T–MoS_2 and monolayer MoS_2. In view of the enhancement in the HER of nano-structured MoS_2, various intercalation techniques have been employed to extend the interlayer space and to increase the active sites of MoS_2 specimens. Compared with intercalations of graphene oxide and some other materials, the process of polymer intercalation can be easily performed. To the best of our knowledge, however, as for the improvement in HER of MoS_2-based catalyst, insufficient efforts for the intercalation of polymers have been devoted to the increase in the exposed unsaturated edge sites and the reduction in the stacked thickness. Thus, the enhancement in HER of MoS_2 catalyst merits extensive exploration.

The aim of this study is to reveal the effects of intercalated polymers on the structure, density of active edge sites, and HER activity of nanoflower-like MoS_2. Thus, three polymers, *i.e.*, polyvinylpyrrolidone (PVP), polyvinyl alcohol (PVA), and polyethylenimine (PEI) were added to the

aqueous solutions employed for the fabrication of nanoflower-like MoS_2 via a solvothermal synthesis approach. Herein, the prepared MoS_2 specimens were characterized using scanning electron microscope (SEM), transmission electron microscopy (TEM), X-ray diffraction (XRD), as well as Raman and Fourier transform infrared spectroscopy (FTIR). The electrocatalytic performances in HER of theses lamellar catalysts were evaluated by the techniques of linear sweep voltammetry (LSV) and electrochemical impedance spectroscopy (EIS). This work sheds insight into the enhancement in HER of the MoS_2-based material.

2. Material and Methods

2.1. Material

Analytical grade reagents of ammonium molybdate tetrahydrate ($(NH_4)_6Mo_7O_{24}{\cdot}4H_2O$, AHM, 99 wt. %), thiourea (CH_4N_2S, 99 wt. %), polyvinyl alcohol (PVA, average molecular weight of 77087.5, 93 wt. %), polyethylenimine (PEI, average molecular weight of 600, 99 wt. %), polyvinylpyrrolidone (PVP, average molecular weight of 10,000, 95 wt. %), and sulfuric acid (H_2SO_4, 98 wt. %) were purchased from Jingchun Scientific Co. Ltd. (Shanghai, China). The 5 wt. % of Nafion solution was provided by Alfa Aesar Chemicals Co. Ltd. (Shanghai, China). The above mentioned reagents were used as received and without further purification.

2.2. Synthesis of Nanoflower-Like MoS_2

The preparation process of nanoflower-like MoS_2 was as follows: 1.41 g of AHM and 0.26 g of thiourea were dissolved in 20 mL of distilled water, and the mixed solution was stirred to form a homogeneous solution. Then, a certain amount of polymer (PVA in the range of 0.04–0.4 g/g MoS_2, PVP in the range of 0.08–2.0 g/g MoS_2, PEI in the range of 0.04–0.4 g/g MoS_2) was added to the mixed solution. This solution was stirred for another 30 min at room temperature to guarantee the homogeneity of the solution. Afterward, the mixed solution was transferred to a 25 mL Teflon-lined stainless steel autoclave placed in an electric cooker (WRN-010, Eurasian, Tianjin, China). Then the temperature of this mixed solution was increased to 200 °C and maintained for 24 h. When the temperature of the solution naturally cooled from 200 °C to room temperature, the solution was centrifuged and then washed with distilled water and ethanol to remove residual reactants. Finally, the obtained powders were dried at 60 °C under a vacuum atmosphere. With the addition of PVA, PVP, and PEI, the prepared samples were described as MoS_2/(PVA)–X, MoS_2/(PVP)–X and MoS_2/(PEI)–X (Table 1), respectively; where X denotes the concentration of polymer (g/g MoS_2) in the solution. Without the presence of polymer, the pure MoS_2 was fabricated by a similar process to that mentioned above.

Table 1. Additions of reagents for MoS_2/polymers catalysts with the hydrothermal synthesis process. Polyvinyl alcohol (PVA), polyvinylpyrrolidone (PVP), polyethylenimine (PEI), Thiourea, ammonium molybdate tetrahydrate (AHM) and H_2O are listed.

Sample	PVA (g/g MoS_2)	PVP (g/g MoS_2)	PEI (g/g MoS_2)	Thiourea (g)	AHM (g)	H_2O (mL)
Pure MoS_2	–	–	–	0.26	1.41	20
MoS_2/PVA–0.04	0.04	–	–	0.26	1.41	20
MoS_2/PVA–0.2	0.2	–	–	0.26	1.41	20
MoS_2/PVA–0.4	0.4	–	–	0.26	1.41	20
MoS_2/PVP–0.08	–	0.08	–	0.26	1.41	20
MoS_2/PVP–0.4	–	0.4	–	0.26	1.41	20
MoS_2/PVP–2.0	–	2.0	–	0.26	1.41	20
MoS_2/PEI–0.04	–	–	0.04	0.26	1.41	20
MoS_2/PEI–0.2	–	–	0.2	0.26	1.41	20
MoS_2/PEI–0.4	–	–	0.4	0.26	1.41	20

2.3. Characterization

An X-ray diffractometer (XRD, Smartlab, Tokyo, Japan) with a Cu Kα radiation (λ = 1.5418 Å) was employed to investigate the structures of the prepared catalysts. Raman spectroscopy was conducted using a Raman Microscope (E55+FRA106, Bruker, Karlsruhe, Germany) with an excitation wavelength of 514.5 nm. The morphology analysis was performed using a scanning electron microscope (SEM, S-4800, Hitachi, Tokyo, Japan) with an accelerating voltage of 5 kV. Transmission electron microscopy (TEM) and high resolution TEM (HRTEM) images were performed with a microscope (JEM-2010, JEOL, Tokyo, Japan) at a voltage of 200 kV. A Nicolet iS5 Fourier transform infrared spectrometer (Thermo Fisher Scientific, Madison, WI, USA) was adopted to determine the FTIR spectra of the specimens with 16 scans at a resolution of 4 cm^{-1} interval.

2.4. Fabrication of the Electrodes

The fabrication process of the tested electrode was described as follows. First, 5 mg of pure MoS_2 or MoS_2/polymer powder and 30 μL of Nafion solution (5 wt. %) were dispersed in 1 mL of ethanol-water solution at room temperature (the volume ratio between absolute ethanol and distilled water is 1:3). Then the mixed solution was dispersed for 1 h using an ultrasonic cleaner (YJ5120-10, Kun Shan Ultrasonic Instruments Co. Ltd., Kunshan, China). Second, 5 μL of the dispersed solution was dropped onto the surface of a glassy carbon electrode (GCE) with a diameter of 3 mm (Aida Hengsheng Technology Co. Ltd., Tianjin, China). Finally, the modified GCE with a powder loading of 0.34 mg/cm^2 was dried at room temperature for 24 h. The obtained electrodes were denoted as MoS_2/PVA–X, MoS_2/PVP–X and MoS_2/PEI–X (Table 1), where X denotes the different addition of PVA, PVP, and PEI. The pure MoS_2 electrode was fabricated exactly as the above process, except for pure MoS_2 powder applied to replace the MoS_2/polymer powder.

2.5. Electrochemical Measurements

All the electrochemical measurements were performed in a 0.5 $mol \cdot L^{-1}$ H_2SO_4 solution at 298 K under atmospheric pressure, using an electrochemical workstation (CHI 650C, Chenhua Co. Ltd., Shanghai, China). A three stand electrode cell was employed, where the fabricated electrode mentioned above, Ag/AgCl, and Pt wire were employed as working electrode, reference electrode, and auxiliary electrode. Before the tests, all the electrolytes were deaerated by purging with pure N_2 gas for 40 min before the tests.

Linear sweep voltammetry (LSV) was conducted between −0.25 and 0.1 V at 2 $mV \cdot s^{-1}$. Electrochemical impedance spectroscopy (EIS) was measured at a cathode overpotential of 200 mV; the employed amplitude of the sinusoidal signal was 5 mV. All EIS tests were always carried out from high frequency to low frequency, and the frequency ranged from 10^5 to 10^{-2} Hz. During the test, all potentials were collected *versus* the Ag/AgCl electrode. Then the potentials (*versus* Ag/AgCl) were calibrated to a reversible hydrogen electrode (RHE) as follows: $E_{RHE} = E_{Ag/AgCl} + 0.059pH + 0.209$ V. All the measurements were performed in triplicate to guarantee the reproducibility of the experimental data.

3. Results and Discussions

3.1. Characterization of Nanoflower-Like MoS_2

3.1.1. X-Ray Diffraction (XRD) Spectra

The XRD patterns of the prepared MoS_2-based nanoflower-like samples are presented in Figure 1. For the purpose of comparison, the standard pattern of the pristine 2H-MoS_2 (JCPDS No. 37-1492) is also displayed within Figure 1. Three peaks appearing at $2\theta = 15.0°$, 33.8°, and 57.1° correspond to the (002), (100), and (110) planes of the pristine 2H–MoS_2, respectively. It is noteworthy that, compared to that of pure MoS_2, the locations of the composites corresponding to the (002) peaks shift to lower angles. The diffraction peaks of composites centered at around $2\theta = 12.5°$ correspond to the interspacing (*d*) of 7.08 Å obtained via the Bragg equation. Herein, the interspacing thicknesses of the three MoS_2 composite specimens are identical, which may be due to the low additions of PVA, PVP, and PEI. The interspacing of 7.08 Å for MoS_2/polymer composites is much larger than that of the pure MoS_2 (5.9 Å), indicating the expansion of lattice and the intercalation of polymers [26,27]. In addition, the weak characteristic of these three peaks for the prepared samples is validated, suggesting their poor crystallizations. Meanwhile, with a decrease in concentrations of polymers, the shapes of these reflection peaks become sharper, suggesting enhancement of crystallinities. It is noteworthy that the decline of the (002) diffraction peak indicates a low stacking height [28], which is effective for offering more active sites and lower intrinsic resistance for HER [21].

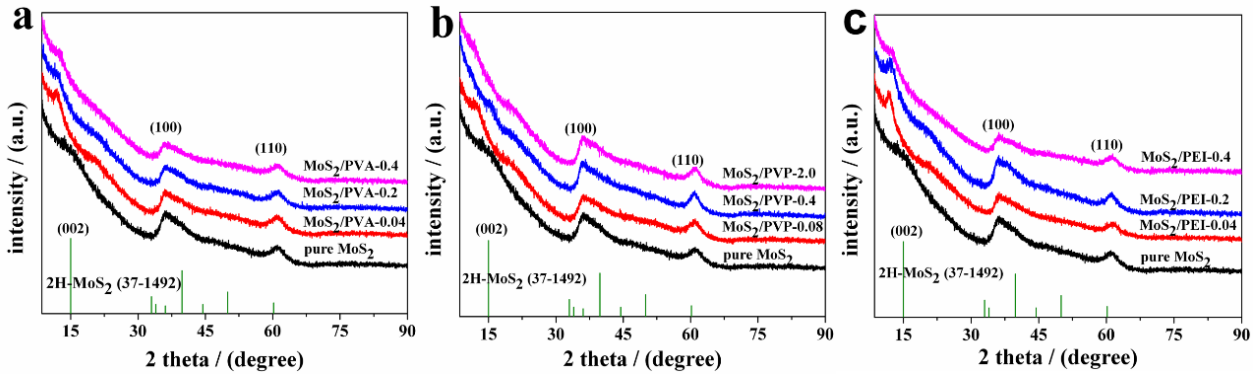

Figure 1. X-ray diffraction (XRD spectra of the as-prepared MoS_2-based nanoflower-like catalysts: (**a**) MoS_2/polyvinyl alcohol (PVA) composite; (**b**) MoS_2/polyvinylpyrrolidone (PVP) composite; (**c**) MoS_2/polyethylenimine (PEI) composite.

3.1.2. Raman Spectra

The Raman spectra of MoS_2/PVA composites are reported in Figure 2a. The two characteristic peaks of pure MoS_2 at 372 and 402 cm^{-1} match well with the E_{2g}^1 and A_{1g} vibrational models of the hexagonal MoS_2 [29]. With the increase in concentration of PVA, intensities of E_{2g}^1 and A_{1g} peaks become low and weak, demonstrating the decrease in crystallinities of the composites. Herein, Raman spectra of MoS_2/PVP and MoS_2/PEI composites with different additions of PVP and PEI are not given, because of their similarities to that of MoS_2/PVA. In general, the difference in frequency between E_{2g}^1 and A_{1g} is helpful in determining the number of stacked layers [30,31]. As demonstrated in Figure 2a,b, for MoS_2/PVA, MoS_2/PVP, MoS_2/PEI composites, a red shift of the E_{2g}^1 band and a blue shift of the A_{1g} band are observed; thus the smaller differences between E_{2g}^1 and A_{1g} can be validated for these three composites. In contrast with that of pure MoS_2, we confirmed that the intercalations of polymers reduce the stacking thicknesses of the nanoflower-like MoS_2 composites. It should be pointed out that Raman spectra of the composite specimens strongly depend on the stoichiometry of their components, thus the different HER activity between the pure MoS_2 and the composites might be confirmed.

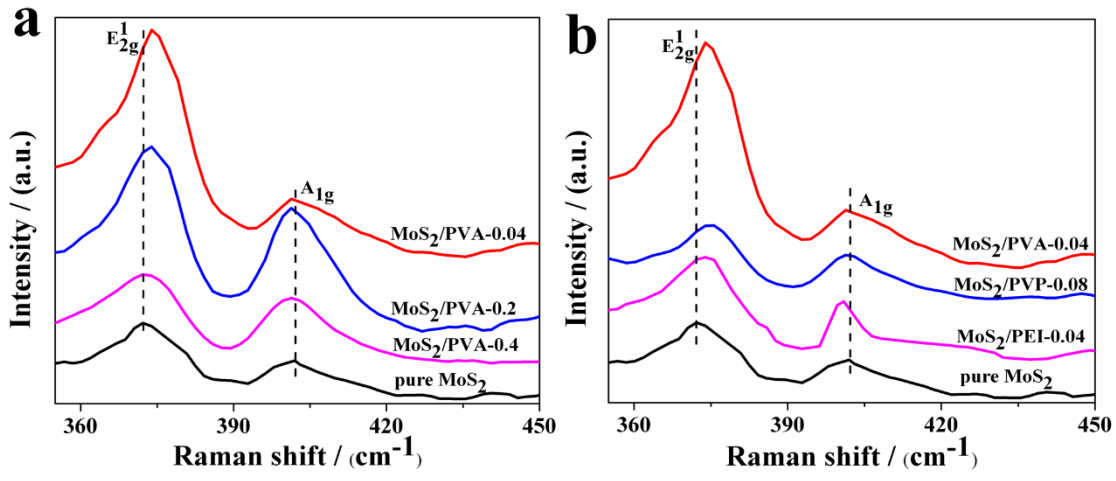

Figure 2. Raman spectra of various MoS_2-based nanoflower-like catalysts: (**a**) MoS_2/PVA composite; (**b**) MoS_2/PVA–0.04, MoS_2/PVP–0.08, and MoS_2/PEI–0.04 composites.

3.1.3. FTIR Spectra

FTIR spectra of MoS_2/PVA composites (Figure 3a), MoS_2/PVP composites (Figure 3b), and MoS_2/PEI (Figure 3c) composites were measured. As shown in Figure 3, the strong absorbance peaks appearing at 3000 to 3600 cm^{-1} indicate the presences of intermolecular and intramolecular hydrogen bonds; nevertheless, to some extent, these peaks are overlapped by the absorbance of water molecules. The characteristic peaks of O–H, CH_2, and C–H groups for PVA (Figure 3a) with the wave number in the range of 1330–1648 cm^{-1} can be observed [32], while the peaks of the C–O stretch and O–H bending can be found at 1096 cm^{-1}. The characteristic peaks of the MoS_2/PVA composites are consistent with that of pure PVA. As for the pure PVP and MoS_2/PVP composites (Figure 3b), the peaks corresponding to C=O stretching vibration, and C–N stretching vibration are observed at 1659 cm^{-1}, and 1284 cm^{-1} [33]. The peak located at 3380 cm^{-1} (Figure 3c) corresponds to the $–NH_2$ group in PEI. In addition, peaks appearing at 2948, 2840, and 1459 cm^{-1} can be assigned to asymmetric stretching vibrations of C–H bond, while the peak at 1106 cm^{-1} is attributed to the stretching vibration of the C–N group [34]. Thus, the MoS_2/PVP and MoS_2/PEI composites present the same characteristic peaks as the pure PVP and PEI polymers. Based on the above analyses, the existence of PVA, PVP, and PEI can be validated, thereby indicating theses three polymer molecules can be intercalated in the MoS_2 gallery space during the hydrothermal process.

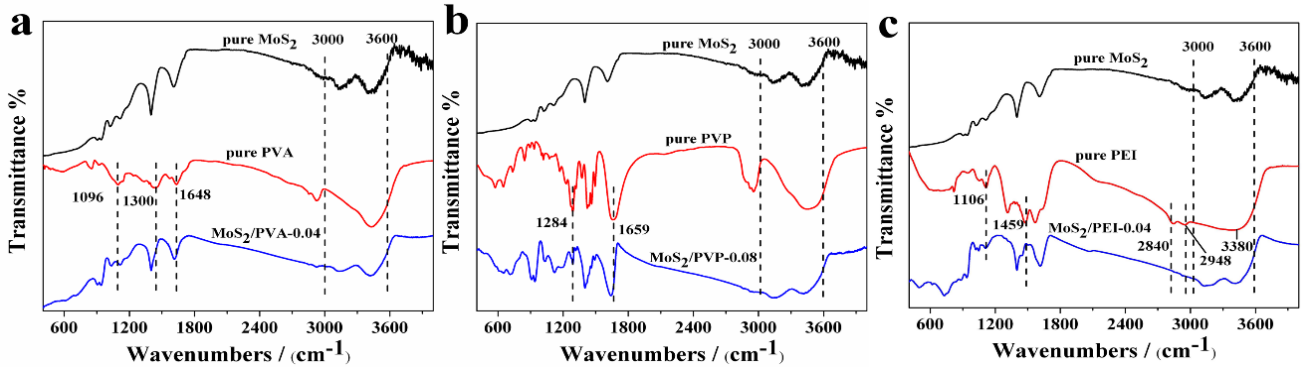

Figure 3. Raman and Fourier transform infrared spectroscopy (FTIR) spectra of (**a**) MoS_2/PVA–0.04 composite; (**b**) MoS_2/PVP–0.08 composite; (**c**) MoS_2/PEI–0.04 composite.

3.1.4. SEM Morphologies

The morphologies of the pure MoS_2 and the synthesized MoS_2/PVA composites are illustrated in Figure 4. All samples are assembled by the lamellar nanoflower-like MoS_2 with diverse lateral sizes ranging from 100 to 400 nm. With the increase in PVA addition (Figure 4b–d), large nano-size flowers with vague edges can be found, suggesting insufficient crystallization of these composites, consistent with the results of XRD. It should be noted that a similar tendency in the presence of PVP and PEI can also be confirmed (Figure 5). Among the MoS_2/polymer composite samples, the MoS_2/PVA–0.4, MoS_2/PVP–2.0 and MoS_2/PEI–0.4 samples exhibit remarkable aggregations (Figures 4d and 5c,f), which may be attributed to the excessive adsorption of polymers at the surface and edge sites of the MoS_2 composites. In addition, with the decrease in polymer addition, the edges of MoS_2 composites

(Figures 4b and 5a,d) can be easily observed, thereby indicating the high crystallinity of the samples. Therefore, a nanoflower-like MoS_2 sample with a high crystallinity and small particle size can be obtained with low additions of polymers (0.04 g/g MoS_2 for PVA and PEI, and 0.08 g/g MoS_2 for PVP).

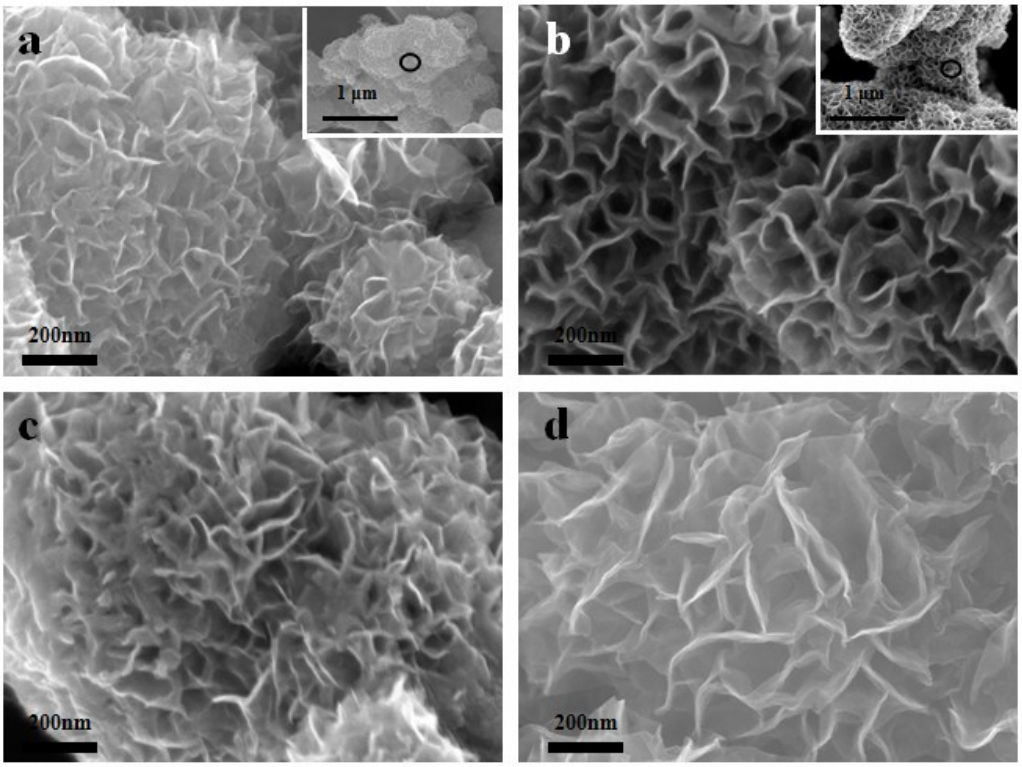

Figure 4. Scanning electron microscope (SEM) images of (**a**) pure MoS_2; (**b**) MoS_2/PVA–0.04 composite; (**c**) MoS_2/PVA–0.08 composite; and (**d**) MoS_2/PVA–0.4 composite.

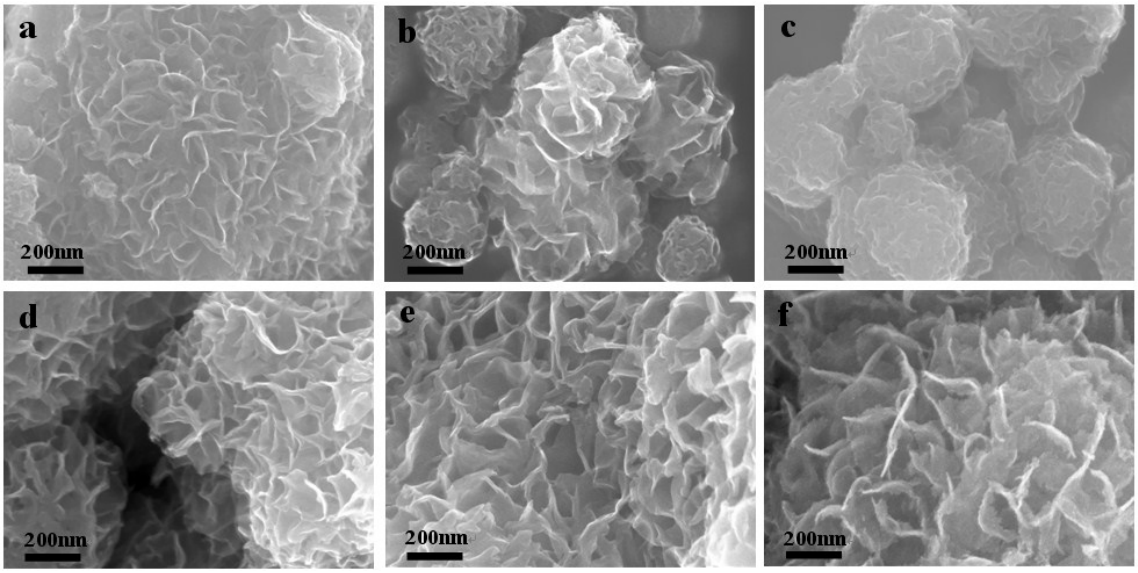

Figure 5. SEM images (**a**–**f**) of the MoS_2/polymer composites synthesized at various concentrations, where **a**–**f** represent MoS_2/PVP–0.08, MoS_2/PVP–0.4, MoS_2/PVP–2.0, MoS_2/PEI–0.04, MoS_2/PEI–0.2, and MoS_2/PEI–0.4 composites.

3.1.5. TEM

To further elucidate the morphologies of the obtained composites, transmission electron microscopy (TEM) and high-resolution TEM (HRTEM) measurements were performed. From the fabricated composites, MoS_2/PVA–0.04, MoS_2/PVP–0.08, and MoS_2/PEI–0.04 three samples were selected for the tests. Also, the pure MoS_2 sample was analyzed for comparison. As displayed in Figure 6, these samples with a diameter of about 100 nm are assembled by lamellar MoS_2 powders. Nano-size flowers with a thickness of 2–5 nm can be observed, which are notably thinner than that of the pure MoS_2 (~10 nm). The lattice inter spaces of 7.08 Å for MoS_2/PVA–0.04, MoS_2/PVP–0.08 and MoS_2/PEI–0.04 composites are much larger than that of pure MoS_2 (5.9 Å), which is also consistent with the results of XRD. This may be attributed to the intercalations of polymers, and the interactions between the oxygen-containing functional groups of the polymers and the MoS_2 precursors [19]. Thus, the polymers intercalated into the MoS_2 interlayer can afford a number of exposed edges for HER.

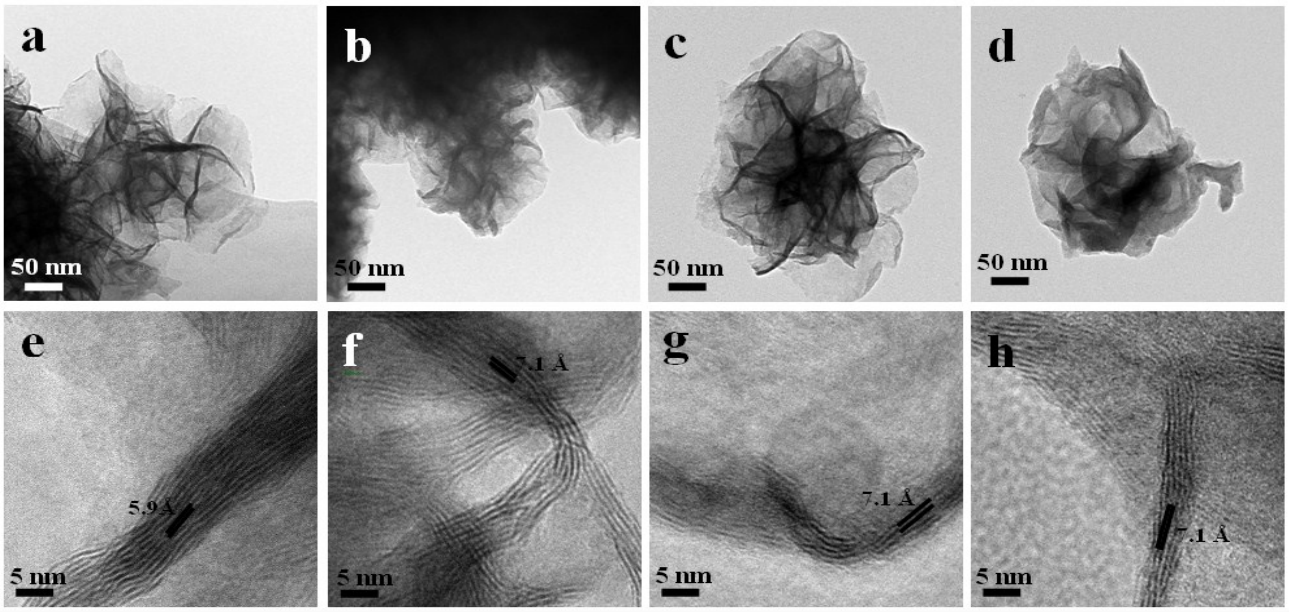

Figure 6. Transmission electron microscopy (TEM) (**a**–**d**) and high resolution transmission electron microscopy (HR-TEM) (**e**–**h**) of the various samples, represented for pure MoS_2, MoS_2/PVA–0.04, MoS_2/PVP–0.08, and MoS_2/PEI–0.04 composites.

3.2. HER Activity of the Nanoflower-Like MoS_2/Polymer

3.2.1. Linear Sweep Voltammetry (LSV)

To evaluate the catalytic activity in HER of the MoS_2/polymer composite, LSV measurements were performed in 0.5 mol·L^{-1} H_2SO_4 solution with a scanning rate of 2 mV·s^{-1} at room temperature. Cathodic polarization curves (Figure 7a) and corresponding Tafel plots (Figure 7d) of MoS_2/PVA–0.04, MoS_2/PVA–0.08, MoS_2/PVA–0.4 were obtained. In comparison with the pure MoS_2 sample, it can be observed that all the MoS_2/PVA composites present much lower onset overpotentials (η); among them, the MoS_2/PVA–0.04 sample exhibits the lowest value of η (~40 mV), suggesting the excellent HER activity. The onset potentials for other MoS_2/PVA composites are in the range of

180–250 mV, these values are still lower than that of the pure MoS_2 (300 mV). As shown in Figure 7a, compared with other specimens, the MoS_2/PVA–0.04 sample exhibits the largest cathodic current density of 20 mA·cm^{-2} at (η = 250 mV), which is 80 times that of the pure MoS_2 (0.25 mA·cm^{-2}). Similarly, the enhancements in HER for MoS_2/PVP and MoS_2/PEI composites can also be validated (Figure 7b,c). The current densities of MoS_2/PVP–0.08 and MoS_2/PEI–0.04 (η = 250 mV) are 9.04 mA·cm^{-2} and 9.60 mA·cm^{-2}, respectively; which are 36-fold and 38-fold levels higher than that of the pure MoS_2.

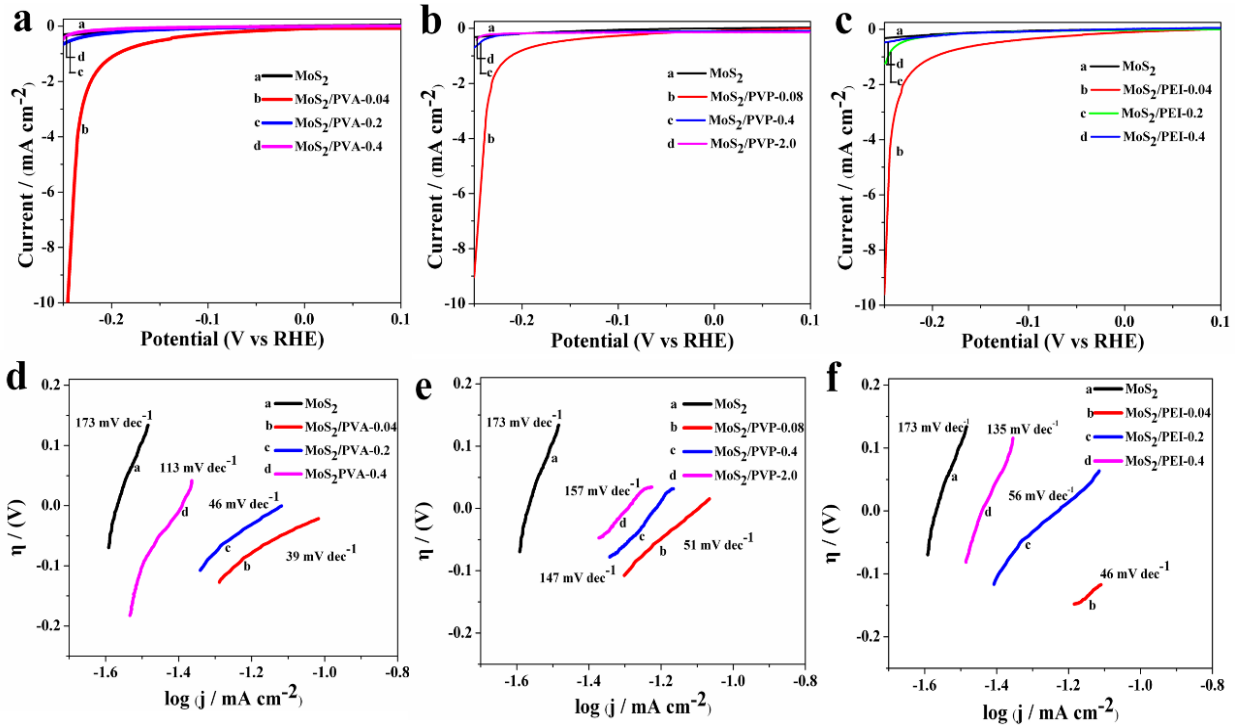

Figure 7. Polarization curves (**a**–**c**) and corresponding Tafel plots (**d**–**f**) of the MoS_2/PVA, MoS_2/PVP, MoS_2/PEI composites.

It is well known that the smaller the Tafel slope of the sample, the higher the HER activity [35,36] will be. The Tafel plots (Figure 7d–f) fit the following Tafel equation:

$$\eta = b \times \log j + a \quad (1)$$

where, η (mV) is the overpotential, and j (mA·cm^{-2}) is the current density. The values of Tafel slope are ~173, ~113, ~46, and ~39 mV·dec^{-1} for MoS_2, MoS_2/PVA–0.4, MoS_2/PVA–0.2, and MoS_2/PVA–0.04, which are very consistent with published reports [37,38]. Among the samples, MoS_2/PVA–0.04 with the smallest Tafel slope exhibits the highest HER activity. The small Tafel plot compares to that of the other reported polymer [39]. Although Tafel slopes of MoS_2/PVA–0.2, MoS_2/PVA–0.4 samples are larger than that of MoS_2/PVA–0.04, their HER activities are still higher than that of the pure MoS_2 because of their smaller Tafel slopes. Similarly, the same can be concluded for MoS_2/PVP and MoS_2/PEI composites. Among these two kinds of composite, the MoS_2/PVP–0.08 and MoS_2/PEI–0.04 samples possess notable HER activities due to smaller Tafel slopes than those of other corresponding samples (Figure 7e,f). However, these two composites for HER activity are inferior to the MoS_2/PVA–0.04 sample.

Based on the above mentioned results, we realize that all the prepared composites present quite different HER activities due to the effects of different concentrations of polymers. Considering the feasibilities of intercalation polymers in the interlayer of MoS_2 catalysts and excessive adsorption of them on the surface and edge sites of MoS_2, the HER activities of these three kinds of composites are reduced with increase in the additions of the polymers. Thus, the enhancement in HER for nanoflower-like MoS_2 can be achieved by adjusting the polymer addition.

3.2.2. Electrochemical Impedance Spectroscopy (EIS)

The kinetics of MoS_2/polymer composites in HER can be further illustrated by EIS, and the results are reported in Figure 8. The EIS data were fitted using a modified Randles equivalent circuit shown in Scheme 1. The values of the circuit elements obtained by fitting the experimental results are shown in Table 2. Herein, a constant phase element (CPE) was adopted to model the electrical double layer of the electrode/electrolyte interface. The necessity of CPE in place of pure capacitance is due to the dispersed distribution of Nyquist diagrams in the high frequency domain [40]. The double layer capacitance (C_{dl}) and exchange current density (i_0) of the electrode were estimated using Equations (2) and (3) [41]:

$$C_{dl} = Y_0 \times (R_s^{-1} + R_{ct}^{-1})^{n-1} \quad (2)$$

$$i_0 = \frac{RT}{nFR_{ct}} \quad (3)$$

where, Y_0 (mS·s·cm^{-2}) regarded as a capacity parameter, is the CPE coefficient; the dimensionless CPE exponent (n) is related to the constant phase angle. R_s (Ω·cm^2), and R_{ct} (Ω·cm^2) are the solution resistance, and the charge transfer resistance, respectively.

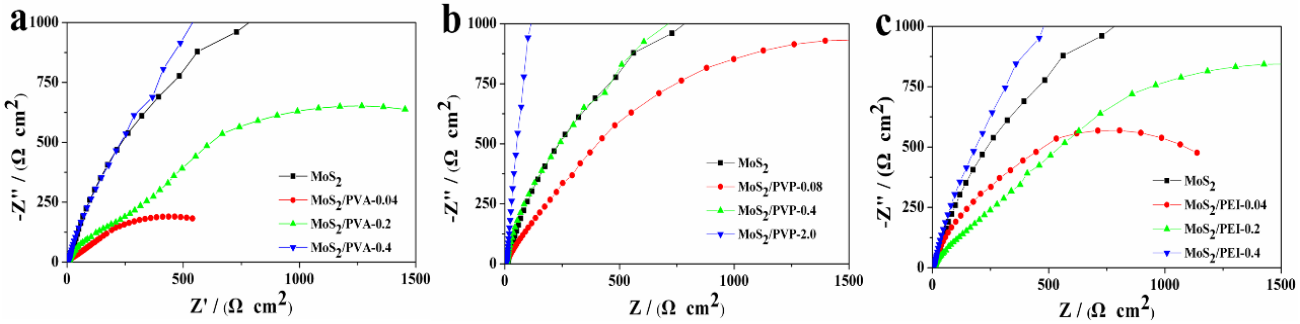

Figure 8. Nyquist plots of MoS_2-based nanoflower-like composite catalysts: (**a**) MoS_2/PVA composite; (**b**) MoS_2/PVP composite; (**c**) MoS_2/PEI composite.

As indicated by Figure 8 and Table 2, compared with that of the MoS_2 pure sample, the Nyquist plots reveal a decrease in charge transfer resistance (R_{ct}) (from 7.55 kΩ·cm^2 to 0.84 kΩ·cm^2), demonstrating the excellent conductivity of the composites (Table 2). R_{ct} of MoS_2/polymer composites follow the sequence of MoS_2/PVA < MoS_2/PEI < MoS_2/PVP. R_{ct} of the MoS_2/PVA–0.04 is smaller than that of other specimens, suggesting a faster charge transfer of this composite. The double layer capacitance (C_{dl}) is calculated to evaluate the exposed active surface area of the electrode. As shown in Table 2, MoS_2/PVA–0.04 exhibits the largest C_{dl} compared to the other ones. Furthermore,

MoS_2/PVA–0.04 exhibits a significant exchange current density (i_0) of 5.89×10^{-5} mA·cm^{-2}, which is 2–11 times larger than that of the other composites. The large i_0 further confirms the excellent activity for HER catalysis. Thus, among the composite samples, the MoS_2/PVA–0.04 composite with the lowest R_{ct}, highest C_{dl} and i_0 provides sufficient active sites, and thereby guarantees excellent HER activity.

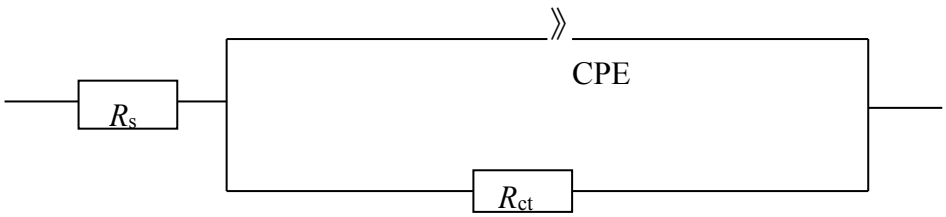

Scheme 1. Randles electrical equivalent circuit compatible with the Nyquist diagrams shown in Figure 8. R_s, R_{ct} and CPE are the solution resistance, the charge transfer resistance, and a constant phase element, respectively.

Table 2. Analyzed parameters of electrochemical impedance spectroscopy (EIS) spectra for the composites.

Sample	R_s/(Ω·cm^2)	R_{ct}/(kΩ·cm^2)	Y_0/(mS·s·cm^{-2})	n	C_{dl}/(mF·cm^{-2})	i_0/(×10^{-5}mA·cm^{-2})
MoS_2	6.13	7.55	0.16	0.67	0.29	0.50
MoS_2/PVA–0.04	4.87	0.84	1.00	0.52	2.13	5.89
MoS_2/PVA–0.2	5.24	1.96	0.25	0.72	0.64	1.82
MoS_2/PVA–0.4	5.86	6.05	0.19	0.79	0.39	0.54
MoS_2/PVP–0.08	5.72	2.62	0.27	0.71	0.85	1.38
MoS_2/PVP–0.4	6.54	3.04	0.20	0.87	0.40	0.97
MoS_2/PVP–2.0	7.58	6.23	0.02	0.81	0.34	0.51
MoS_2/PEI–0.04	6.22	1.45	0.30	0.83	0.87	2.14
MoS_2/PEI–0.2	6.45	2.47	0.21	0.66	0.62	1.58
MoS_2/PEI–0.4	5.71	6.18	0.20	0.80	0.37	0.52

Y_0 regarded as a capacity parameter, is the CPE coefficient. the dimensionless CPE exponent (n) is related to the constant phase angle. R_s and R_{ct} are the solution resistance and the charge transfer resistance. The double layer capacitance (C_{dl}) and exchange current density (i_0) are listed in the table.

3.3. Stability

In addition to the HER activity, stability plays a crucial role in the potential application for a MoS_2-based catalyst. In order to reveal the stability of this catalyst in acidic solution, a long-term cycling test for the MoS_2/PVA–0.04 composite was conducted. This test was performed with the potential ranging from −0.25 to 0.1 V (*vs.* RHE) at a scan rate of 20 mV·s^{-1}. It can be observed that the current density of the composite (Figure 9) shows a slight decrease (less than 4%) after 1000 CV cycles. Thus, the MoS_2/PVA–0.04 composite exhibits excellent durability in the HER process.

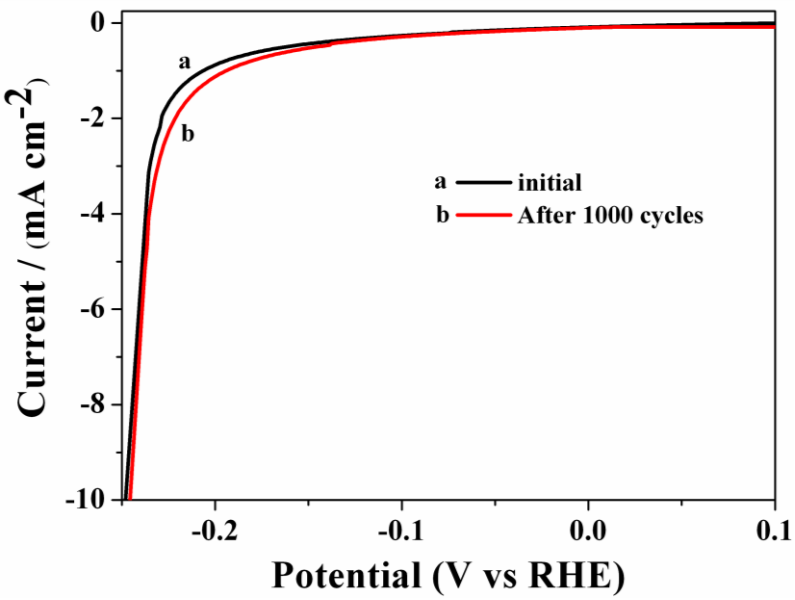

Figure 9. Stability test for the MoS_2/PVA–0.04 composite. RHE = reversible hydrogen electrode.

4. Conclusions

In this study, three kinds of MoS_2/polymer composites were fabricated by a facile hydrothermal method. The effects of three polymers PVA, PVP, and PEI on the stacking height and the quantity of exposed active sites of the nanoflower-like MoS_2 were evaluated. The intercalated or adsorbed polymers provide carbonyl and hydroxyl functional groups for attachment of the MoS_2 precursor, and enlarge the interlayer spacing of MoS_2 particles. The expanded interlayers of nanoflower-like MoS_2 catalysts lead to the enhancement in active sites, resulting in a high electrocatalytic activity for HER. Of all the composites, the MoS_2/PVA–0.04 composite exhibits the best HER activity, due to a small overpotential (~40 mV), a large cathodic current (20 $mA \cdot cm^{-2}$), and a small Tafel slope (~39 $mV \cdot dec^{-1}$).

Acknowledgements

This work was supported by the Scientific Research Foundation of the Hebei Higher Education Institutions of China (Grant No. ZD2015120). Herein, we are also very grateful to the editors and the reviewers for giving the valuable and instructive comments.

Author Contributions

Laizhou Song designed the study. Xianwen Zeng, Lijing Niu, Xiuli Wang, Xuanming Shi and Jiayun Yan performed the experiments. Xianwen Zeng, Lijing Niu and Laizhou Song wrote the paper. Xianwen Zeng, Lijing Niu, and Laizhou Song reviewed and edited the manuscript. All authors read and approved the manuscript.

Conflicts of Interest

The author declares no conflict of interest.

References

1. Mallouk, T.E. Water electrolysis: Divide and conquer. *Nat. Chem.* **2013**, *5*, 362–363.
2. Raimondi, F.; Scherer, G.G.; Kötz, R.; Wokaun, A. Nanoparticles in energy technology: Examples from electrochemistry and catalysis. *Angew. Chem. Int. Ed.* **2005**, *44*, 2190–2209.
3. Liu, Y.; Kelly, T.G.; Chen, J.G.G.; Mustain, W.E. Metal carbides as alternative electrocatalyst supports. *ACS Catal.* **2013**, *3*, 1184–1194.
4. Hinnemann, B.; Moses, P.G.; Bonde, J.; Jørgensen, K.P.; Nielsen, J.H.; Honch, S.; Chorkendorff, I.; Nørskov, J.K. Biornimetic hydrogen evolution: MoS_2 nanoparticles as catalyst for hydrogen evolution. *J. Am. Chem. Soc.* **2005**, *127*, 5308–5309.
5. Dresselhaus, M.S.; Thomas, I.L. Alternative energy technologies. *Nature* **2001**, *414*, 332–337.
6. Antolini, E. Palladium in fuel cell catalysis. *Energy Environ. Sci.* **2009**, *2*, 915–931.
7. Tang, H.; Dou, K.P.; Kaun, C.-C.; Kuang, Q.; Yang, S.H. $MoSe_2$ nanosheets and their graphene hybrids: Synthesis, characterization and hydrogen evolution reaction studies. *J. Mater. Chem. A* **2014**, *2*, 360–364.
8. Chen, Z.B.; Cummins, D.; Reinecke, B.N.; Clark, E.; Sunkara, M.K.; Jaramillo, T.F. Core-shell MoO_3–MoS_2 nanowires for hydrogen evolution: A functional design for electrocatalytic materials. *Nano Lett.* **2011**, *11*, 4168–4175.
9. Cheng, L.; Huang, W.J.; Gong, Q.F.; Liu, C.H.; Liu, Z.; Li, Y.G.; Dai, H.J. Ultrathin WS_2 nanoflakes as a high-performance electrocatalyst for the hydrogen evolution reaction. *Angew. Chem. Int. Ed.* **2014**, *53*, 7860–7863.
10. Vrubel, H.; Merki, D.; Hu, X. Hydrogen evolution catalyzed by MoS_3 and MoS_2 particles. *Energy Environ. Sci.* **2012**, *5*, 6136–6144.
11. Karunadasa, H.I.; Montalvo, E.; Sun, Y.; Majda, M.; Long, J.R.; Chang, C.J. A molecular MoS_2 edge site mimic for catalytic hydrogen generation. *Science* **2012**, *335*, 698–702.
12. Jaramillo, T.F.; Jørgensen, K.P.; Bonde, J.; Nielsen, J.H.; Horch, S.; Chorkendorff, I. Identification of active edge sites for electrochemical H_2 evolution from MoS_2 nanocatalysts. *Science* **2007**, *317*, 100–102.
13. Bonde, J.; Moses, P.G.; Jaramillo, T.F.; Nørskov, J.K.; Chorkendorff, I. Hydrogen evolution on nano-particulate transition metal sulfides. *Faraday Discuss.* **2009**, *140*, 219–231.
14. Liu, N.; Yang, L.C.; Wang, S.N.; Zhong, Z.W.; He, S.N.; Yang, X.Y.; Gao, Q.S.; Tang, Y. Ultrathin MoS_2 nanosheets growing within an *in-situ*-formed template as efficient electrocatalysts for hydrogen evolution. *J. Power Sources* **2015**, *275*, 588–594.
15. Zhou, T.; Yin, H.; Liu, Y.; Chai, Y.; Zhang, J.; Liu, C. Synthesis, characterization and HDS activity of carbon-containing Ni–Mo sulfide nano-spheres. *Catal. Lett.* **2010**, *134*, 343–350.
16. Merki, D.; Vrubel, H.; Rovelli, L.; Fierro, S.; Hu, X. Fe, Co, and Ni ions promote the catalytic activity of amorphous molybdenum sulfide films for hydrogen evolution. *Chem. Sci.* **2012**, *3*, 2515–2525.
17. Jaramillo, T.F.; Bonde, J.; Zhang, J.; Ooi, B.-L.; Andersson, K.; Ulstrup, J.; Chorkendorff, I. Hydrogen evolution on supported incomplete cubane-type $[Mo_3S_4]^{4+}$ electrocatalysts. *J. Phys. Chem. C* **2008**, *112*, 17492–17498.

18. Bian, X.J.; Zhu, J.; Liao, L.; Scanlon, M.D.; Ge, P.Y.; Ji, C.; Girault, H.H.; Liu, B.H. Nanocomposite of MoS_2 on ordered mesoporous carbon nanospheres: A highly active catalyst for electrochemical hydrogen evolution. *Electrochem. Commun.* **2012**, *22*, 128–132.
19. Zheng, X.L.; Xu, J.B.; Yan, K.Y.; Wang, H.; Wang, Z.L.; Yang, S.H. Space-confined growth of MoS_2 nanosheets within graphite: The layered hybrid of MoS_2 and graphene as an active catalyst for hydrogen evolution reaction. *Chem. Mater.* **2014**, *26*, 2344–2353.
20. Li, Y.G.; Wang, H.L.; Xie, L.M.; Liang, Y.Y.; Hong, G.S.; Dai, H.J. MoS_2 nanoparticles grown on graphene: An advanced catalyst for the hydrogen evolution reaction. *J. Am. Chem. Soc.* **2011**, *133*, 7296–7299.
21. Wang, D.Z.; Pan, Z.; Wu, Z.Z.; Wang, Z.P.; Liu, Z.H. Hydrothermal synthesis of MoS_2 nanoflowers as highly efficient hydrogen evolution reaction catalysts. *J. Power Sources* **2014**, *264*, 229–234.
22. Kong, D.S.; Wang, H.T.; Cha, J.J.; Pasta, M.; Koski, K.J.; Yao, J.; Cui, Y. Synthesis of MoS_2 and $MoSe_2$ films with vertically aligned layers. *Nano Lett.* **2013**, *13*, 1341–1347.
23. Tsai, C.; Pedersen, F.A.; Nørskov, J.K. Tuning the MoS_2 edge-site activity for hydrogen evolution via support interactions. *Nano Lett.* **2014**, *14*, 1381–1387.
24. Lukowski, M.A.; Daniel, A.S.; Meng, F.; Forticaux, A.; Li, L.S.; Jin, S. Enhanced hydrogen evolution catalysis from chemically exfoliated metallic MoS_2 nanosheets. *J. Am. Chem. Soc.* **2013**, *135*, 10274–10277.
25. Shi, J.P.; Ma, D.L.; Han, G.-F.; Zhang, Y.; Ji, Q.Q.; Gao, T.; Sun, J.Y.; Song, X.J.; Li, C.; Zhang, Y.S.; *et al.* Controllable growth and transfer of monolayer MoS_2 on Au foils and its potential application in hydrogen evolution reaction. *ACS Nano* **2014**, *8*, 10196–10204.
26. Bissessur, R.; Gallant, D.; Brüning, R. Novel nanocomposite material consisting of poly[oxymethylene-(oxyethylene)] and molybdenum disulfide. *Mater. Chem. Phys.* **2003**, *82*, 316–320.
27. Lin, B.-Z.; Ding, C.; Xu, B.-H.; Chen, Z.-J.; Chen, Y.-L. Preparation and characterization of polythiophene/molybdenum disulfide intercalation material. *Mater. Res. Bull.* **2009**, *44*, 719–723.
28. Wu, Z.Z.; Fang, B.Z.; Wang, Z.P.; Wang, C.L.; Liu, Z.H.; Liu, F.Y.; Wang, W.; Alfantazi, A.; Wang, D.Z.; Wilkinson, D.P. MoS_2 nanosheets: A designed structure with high active site density for the hydrogen evolution reaction. *ACS Catal.* **2013**, *3*, 2101–2107.
29. Wang, H.T.; Lu, Z.Y.; Xu, S.C.; Kong, D.S.; Cha, J.J.; Zheng, G.Y.; Hsu, P.-C.; Yan, K.; Bradshaw, D.; Prinz, F.B.; *et al.* Electrochemical tuning of vertically aligned MoS_2 nanofilms and its application in improving hydrogen evolution reaction. *Proc. Natl. Acad. Sci. USA* **2013**, *110*, 19701–19706.
30. Lee, C.G.; Yan, H.G.; Brus, L.E.; Heinz, T.F.; Hone, J.; Ryu, S. Anomalous lattice vibrations of single and few-layer MoS_2. *ACS Nano* **2010**, *4*, 2695–2700.
31. Yu, Y.F.; Huang, S.Y.; Li, Y.P.; Steinmann, S.N.; Yang, W.T.; Cao, L.Y. Layer-dependent electrocatalysis of MoS_2 for hydrogen evolution. *Nano Lett.* **2014**, *14*, 553–558.
32. Peresin, M.S.; Vesterinen, A.-H.; Habibi, Y.; Johansson, L.-S.; Pawlak, J.J.; Nevzorov, A.A.; Rojas, O.J. Crosslinked PVA nanofibers reinforced with cellulose nanocrystals: Water interactions and thermomechanical properties. *J. Appl. Polym. Sci.* **2014**, doi:10.1002/app.40334.

33. Prasanth, S.; Irshad, P.; Raj, D.R.; Vineeshkumar, T.V.; Philip, R.; Sudarsanakumar, C. Nonlinear optical property and fluorescence quenching behavior of PVP capped ZnS nanoparticles co-doped with Mn^{2+} and Sm^{3+}. *J. Lumin.* **2015**, *166*, 167–175.
34. Popescu, L.M.; Piticescu, R.M.; Petriceanu, M.; Ottaviani, M.F.; Cangiotti, M.; Vasile, E.; Dîrtu, M.M.; Wolff, M.; Garcia, Y.; Schinteie, G.; *et al.* Hydrothermal synthesis of nanostructured hybrids based on iron oxide and branched PEI polymers. Influence of high pressure on structure and morphology. *Mater. Chem. Phys.* **2015**, *161*, 84–95.
35. Merki, D.; Hu, X. Recent developments of molybdenum and tungsten sulfides as hydrogen evolution catalysts. *Energy Environ. Sci.* **2011**, *4*, 3878–3888.
36. Chang, Y.-H.; Nikam, R.D.; Lin, C.-T.; Huang, J.-K.; Tseng, C.-C.; Hsu, C.-L.; Cheng, C.-C.; Su, C.-Y.; Li, L.-J.; Chua, D.H.C. Enhanced electrocatalytic activity of MoS_x on TCNQ-treated electrode for hydrogen evolution reaction. *ACS Appl. Mater. Interfaces* **2014**, *6*, 17679–17685.
37. Xie, J.F.; Zhang, J.J.; Li, S.; Grote, F.; Zhang, X.D.; Zhang, H.; Wang, R.X.; Lei, Y.; Pan, B.C.; Xie, Y. Controllable disorder engineering in oxygen-incorporated MoS_2 ultrathin nanosheets for efficient hydrogen evolution. *J. Am. Chem. Soc.* **2013**, *135*, 17881–17888.
38. Voiry, D.; Salehi, M.; Silva, R.; Fujita, T.; Chen, M.W.; Asefa, T.; Shenoy, V.B.; Eda, G.; Chhowalla, M. Conducting MoS_2 nanosheets as catalysts for hydrogen evolution reaction. *Nano Lett.* **2013**, *13*, 6222–6227.
39. Youssef, L.; Alain, D.; Jean-Claude, M. Electrocatalytic hydrogen evolution from molybdenum sulfide-polymer composite films on carbon electrodes. *ACS Appl. Mater. Interfaces* **2015**, *7*, 15866–15875.
40. Heli, H.; Sattarahmady, N.; Jabbari, A.; Moosavi-Movahedi, A.A.; Hakimelahi, G.H.; Tsai, F.-Y. Adsorption of human serum albumin onto glassy carbon surface—Applied to albumin-modified electrode: Mode of protein-ligand interactions. *J. Electroanal. Chem.* **2007**, *610*, 67–74.
41. Alcaide, F.; Brillas, E.; Cabot, P.-L. EIS analysis of hydroperoxide ion generation in an uncatalyzed oxygen-diffusion cathode. *J. Electroanal. Chem.* **2003**, *547*, 61–73.